Energy & Environmental Science

Supporting materials for

Magnetic Field Induced Capacitance Enhancement in Graphene and Magnetic Graphene Nanocomposites

Jiahua Zhu,[1] Minjiao Chen,[1] Honglin Qu,[1,2] Zhiping Luo,[3] Shijie Wu,[4]
Henry A. Colorado,[5] Suying Wei[2*] and Zhanhu Guo[1*]

[1]Integrated Composites Laboratory (ICL)
Dan F Smith Department of Chemical Engineering
Lamar University, Beaumont, TX 77710 USA

[2]Department of Chemistry and Biochemistry, Lamar University, Beaumont, TX 77710 USA

[3] Department of Chemistry and Physics, Fayetteville State University, Fayetteville, NC 28301 USA

[4]Agilent Technologies, Inc, Chandler, AZ 85226 USA

[5]Department of Mechanical and Aerospace Engineering, University of California Los Angeles, Los Angeles, CA 90095 USA

* Corresponding author

Email: zhanhu.guo@lamar.edu Phone: (409) 880-7654 (Z. G.)

Email: suying.wei@lamar.edu Phone: (409) 880-7976 (S. W.)

S1. TEM and SEM of Graphene and MGNCs

The surface morphology of the electrodes after loading active materials was investigated using SEM. Fig. S1(a&b) shows the layered porous structure of nickel foam with a smooth nickel wire surfaces. Fig. S1(c&d) exhibits the nickel foam (NF) loaded with graphene, it is obvious that the nickel wires are coated by a rough layer of graphene. The area marked with yellow arrows in Fig. S1(c&d) indicates the distribution of graphene. Fig. S1(e&f) reveals the MGNCs coated on the nickel foam. The shining spots as marked with arrow in Fig. S1(f) represent the nanoparticles on the graphene surface. All the evidences reveal that the graphene and MGNCs are strongly adhered to the nickel foam net structure. And also, it is worth to mention that the electroactive materials are stably maintained without peeling off from the NF during testing.

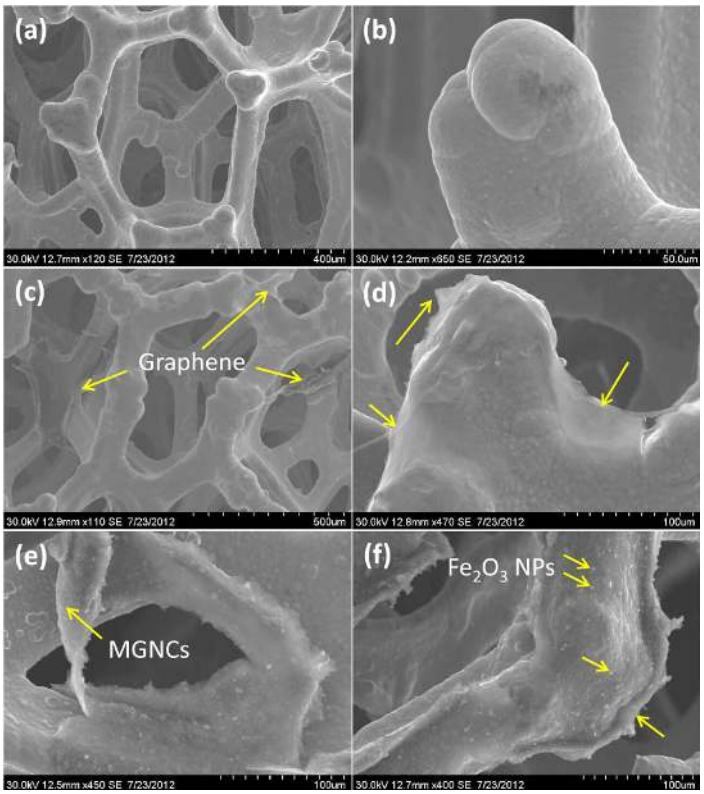

Fig. S1 SEM microstructure of **(a&b)** nickel foam (NF), **(c&d)** NF loaded with graphene, and **(e&f)** NF loaded with MGNCs.

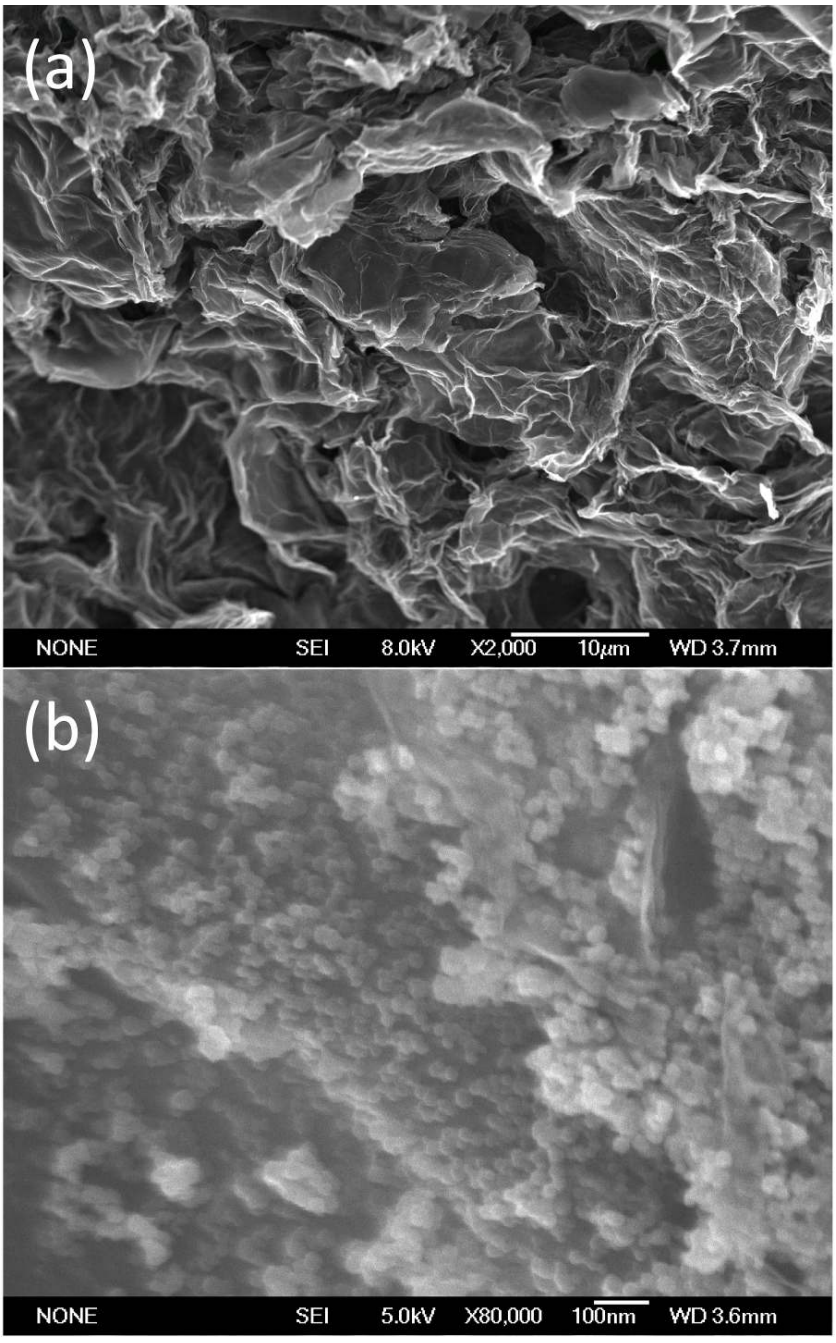

Fig. S2 SEM microstructure of **(a)** graphene and **(b)** MGNCs.

S2. XRD

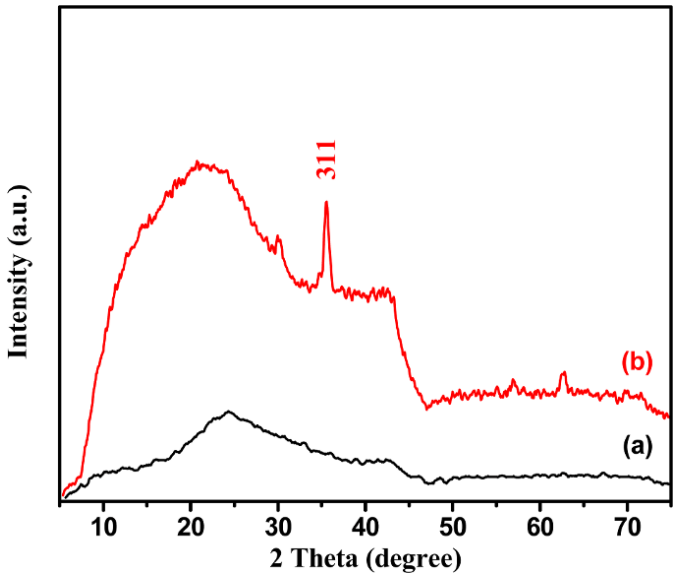

Fig. S3 XRD patterns of **(a)** graphene and **(b)** MGNCs.

Fig. S3 shows the XRD patterns of pure graphene and its MGNCs. The strong additional peak at $2\theta = 35.80^{o}$ is from the (311) crystalline plane of iron oxide (PDF#39-1346). XRD results are well consistent with the HRTEM and SAED results of crystalline Fe_2O_3 nanoparticles.

S3. Magnetization

The magnetic properties of the MGNCs at room temperature are measured in a 9 T physical properties measurement system (PPMS) by Quantum Design.

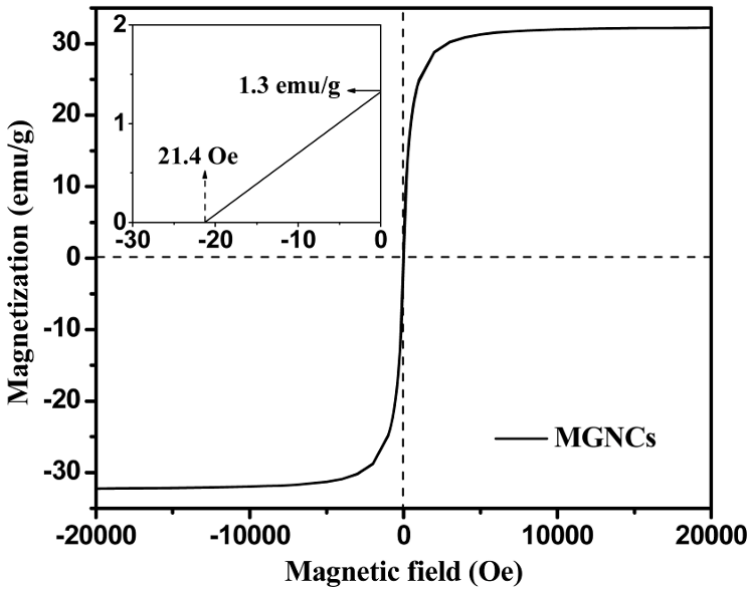

Fig. S4 The room temperature hysteresis loop of the MGNCs.

The M_s of MGNCs is 32.3 emu/g as observed in Fig. S4. Considering the weight ratio of NPs in the MGNCs, the magnetization of pure Fe_2O_3 NPs is calculated to be 61.5 emu/g, which is quite consistent with the theoretical value of γ-Fe_2O_3 (64.0 emu/g[1]).

S4. XPS

The XPS analysis for both graphene and MGNCs is shown in Fig. S5. The results are summarized in Table S1. The C/O atomic ratio for graphene and MGNCs is 5.95 and 5.86, respectively, which indicate that the reduction degree is similar in graphene and MGNCs. The slightly lower C/O ratio of MGNCs is attributed to the existence of metal oxides.

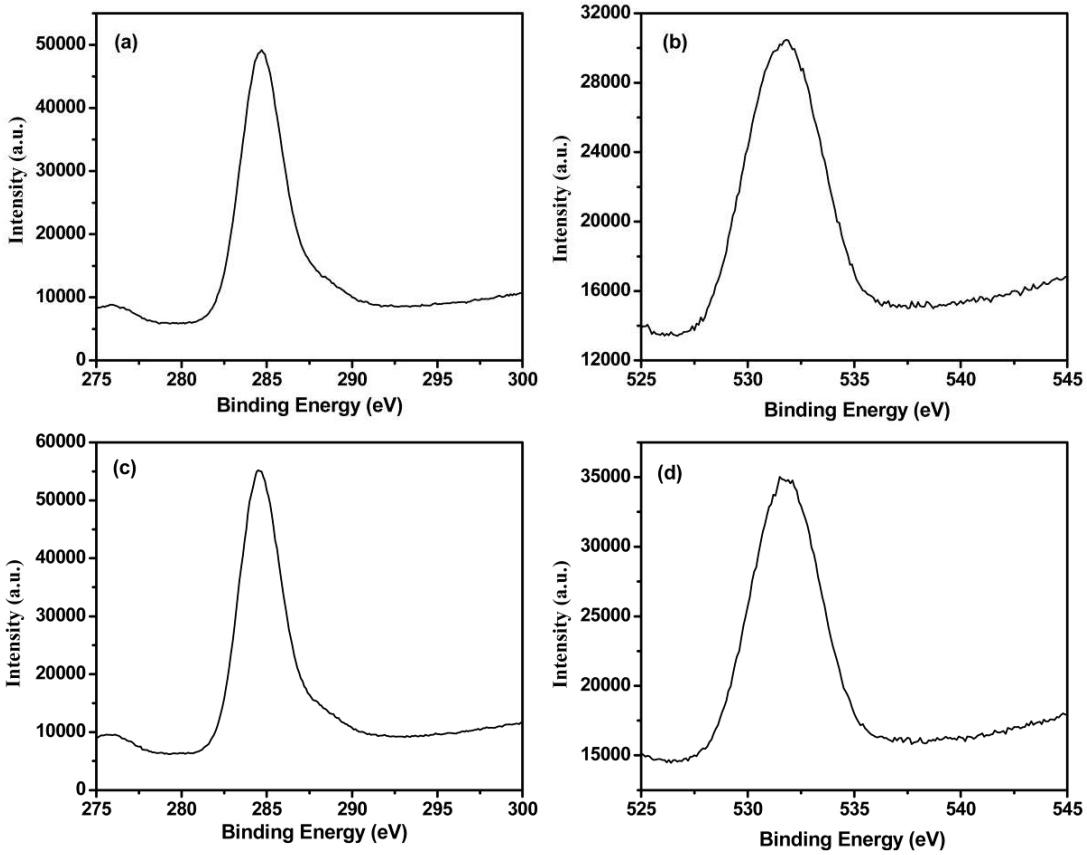

Fig. S5 XPS spectra of graphene **(a)** C1s, **(b)** O1s and MGNCs **(c)** C1s, **(d)** O1s.

Table S1. Atomic and mass concentration of graphene and MGNCs.

Sample	C (atom %)	O (atom %)	C (mass %)	O (mass %)
Graphene	83.98	14.11	79.98	17.89
MGNCs	83.24	14.20	77.29	17.57

S5. Conductivity measurement

The electrical conductivity is tested using four probe technique and the I-V curves are shown in Fig. S6. The electrical resistivity can be calculated using following Equation (S1):[2], [3]

$$\rho = \frac{V \times 2\pi}{I \times (\frac{1}{S_1} + \frac{1}{S_2} - \frac{1}{S_1 + S_2} - \frac{1}{S_2 + S_3}) \times CF} \quad \text{(S1)}$$

where, V (V) is the potential difference between the two inner probes, I (A) is the electrical current that flows through the outer pairs of probes, S_n (mm) represents the distances between the two adjacent probes and CF is the correction factor that depends on W (mm) and S_n. In this case, the resistivity is measured after placing the test piece on a non-conducting surface. This corresponds to the seventh case reported by Valdes,[2] for which the correction coefficient factor is shown in Equation (S2).

$$CF = 1 + 4\frac{S}{W}\sum_{n=1}^{\infty}\left(\frac{1}{\sqrt{\left(\frac{S}{W}\right)^2 + 4n^2}} - \frac{1}{\sqrt{\left(\frac{2S}{W}\right)^2 + 4n^2}}\right) \quad \text{(S2)}$$

where, S is the average distance among the probes, W is the thickness of the test piece.

The electrical resistivity is calculated to be 14.1 and 73.4 Ω·cm for graphene and MGNCs, respectively.

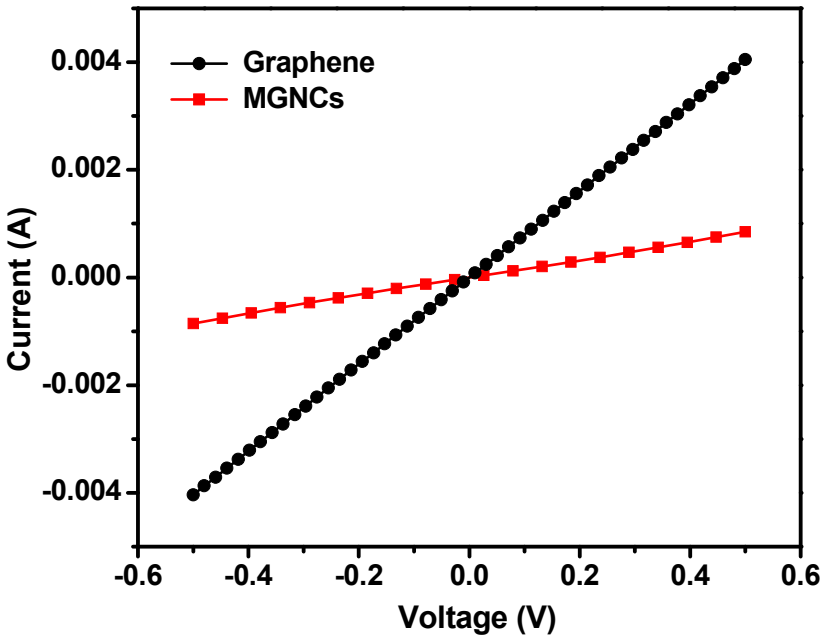

Fig. S6 I-V curves of graphene and MGNCs using four point probe technique.

S6. TGA

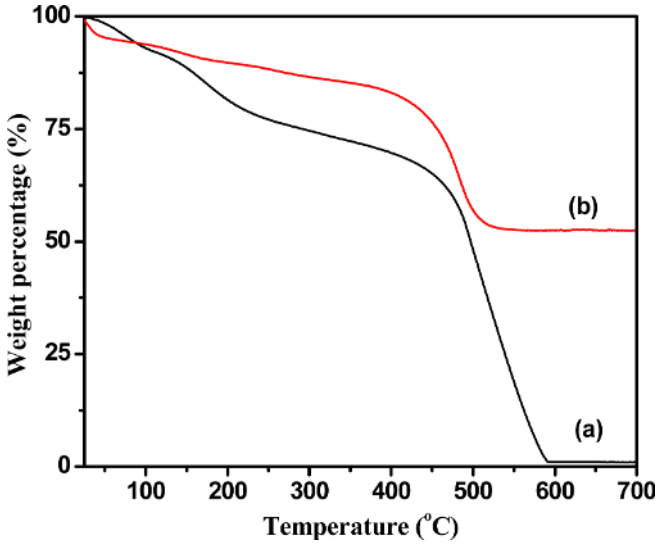

Fig. S7 TGA curves of (a) pure graphene and (b) MGNCs.

Fig. S7 shows the TGA curves of pure graphene and its MGNCs up to 700 ^{o}C in air. The graphene shows a slight weight loss between 300 and 550 ^{o}C, which comes from the residue solvent evaporation and the decomposition of graphene continues until 593 ^{o}C. Different from the graphene curve, the magnetic graphene nanocomposite curve shows a weight loss until 550 ^{o}C due to the decomposition of graphene. The final residue of Fe_2O_3 is 52.5 wt% and the MGNCs comprise 47.5wt% graphene.

S7. Electrochemistry

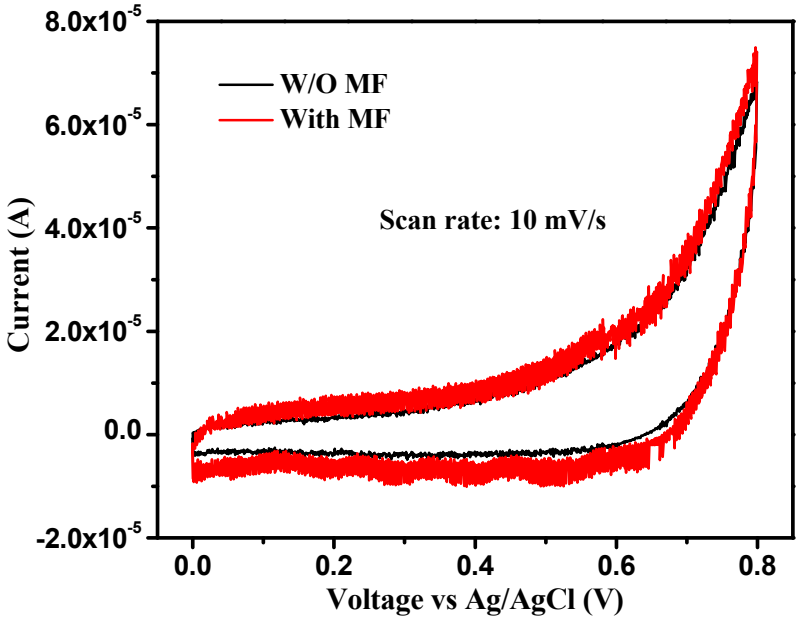

Fig. S8. CV loops of nickel foam at the voltage scan rate of 10 mV/s.

The capacitor performance of NF is tested using cyclic voltammetry, Fig. S8. The CV curve of the NF circles a lunular area, which is not a typical electrostatic capacitor behavior. In addition, the current is very small (~10^{-6} A, the current density can not be calculated since no electroactive material is loaded) as compared to the current after loading electroactive materials (~10^{-4} A, converted from current density in Fig 6b in the paper), which means that the contribution of the capacitance from NF could be neglected after loading electroactive materials. After applying a small external MF (720 G), the CV curve of NF expands and encloses more area following a similar curve pattern without MF. Compared to the huge difference after applying MF in graphene and MGNCs, such a small change is negligible and is not considered in this research.

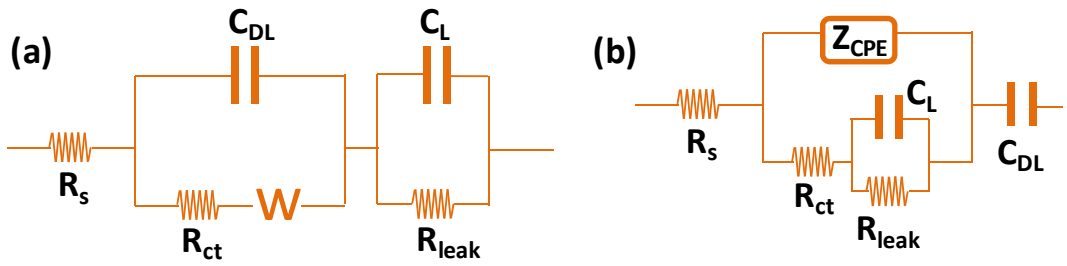

Fig. S9. Equivalent circuit for simulating the impedance spectra of the **(a)** graphene and **(b)** MGNCs electrode, respectively.

The EIS curve with a semicircle at high frequency and straight line at low frequency reveals a capacitor character rather than resistor. Notice that the impedance of a resistor is independent of frequency and has no imaginary component. With only a real impedance component, the current through a resistor stays in phase with the voltage across the resistor. Different equivalent circuit models have been used to simulate the impedance spectra of graphene and MGNCs, since these two electrodes exhibit significantly different EIS spectra, Fig. S9. R_s is the bulk solution resistance, R_{ct} is the charge transfer resistance, R_{leak} is the low frequency leakage resistance, C_{DL} is the double layer capacitance, C_L is the low frequency mass capacitance. W (Warburg element) represents the impedance of semi-infinite diffusion to/from flat electrode. Z_{CPE} is the constant phase element, which indicates the impedance of a capacitor. The simulated resistance results of the two electrodes with/without magnetic field are summarized in Table S2. As can be seen, the solution resistance R_s is very close to each other for both systems independent of the magnetic field. However, the R_{ct} of the MGNCs is significantly larger than graphene, indicating a larger charge transfer resistance at the electrode/electrolyte interface due to the larger resistance of the MGNCs than that of graphene. After applying a small magnetic field, R_{ct} of MGNCs is significantly reduced from 262.1 to 59.4 Ω, which contributes to the improved capacitance in magnetic field.

R_{leak} represents a small leakage current at the electrode/electrolyte interface. The presence of such a large leakage resistance (>4000 Ω)[4] in parallel with the capacitance suggests that the interface undergoes relaxation processes at very low frequencies. After applying the magnetic field, R_{leak} for both graphene and MGNCs are significantly increased, indicating that the interface relaxation has been well restricted and thus improved the electrode capacitance.

Table S2. Power fit of the equivalent circuit model.

	R_s/Ω	R_{ct}/Ω	R_{leak}/Ω
Graphene (W/O MF)	4.6	17.2	4448
Graphene (With MF)	4.2	17.3	4625
MGNCs (W/O MF)	3.2	262.1	9046
MGNCs (With MF)	3.9	59.4	21000

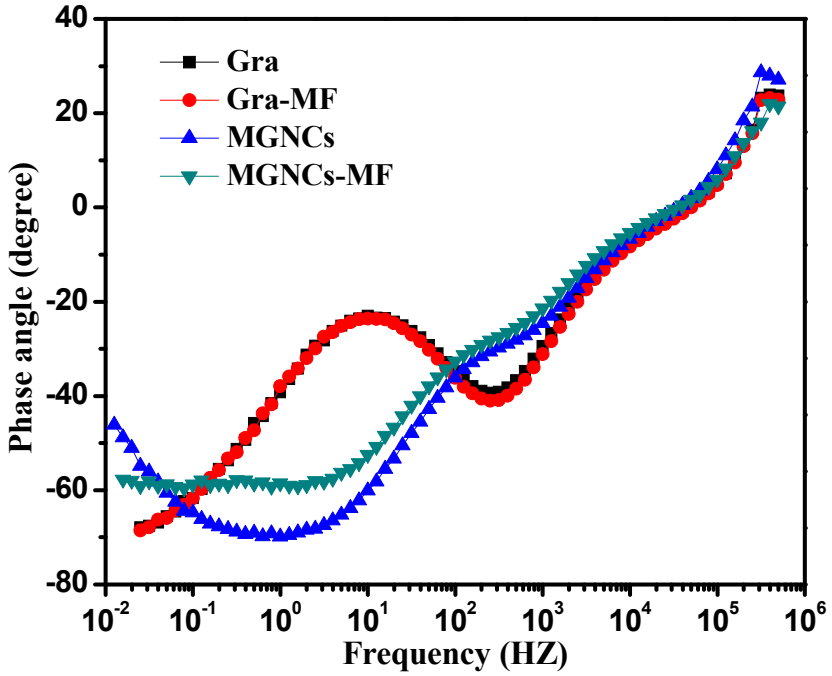

Fig. S10. The phase angle of graphene and MGNCs with and without MF.

The phase angle of the electrode materials in and out of MF is shown in Fig. S10. At low frequency, the phase angle of graphene reaches -70^{o} in the 0.01 Hz region, the values of phase angle are close to that of an ideal capacitor (-90^{o}). With increasing frequency, the phase angle of graphene increases and reaches a peak around 10 Hz. After that, the phase angle curve goes to a valley bottom at ~300 Hz and goes up again till 10^6 Hz. The external magnetic field does not affect the phase angle curve significantly and both curves are almost overlapped. With regards to MGNCs, the phase angle curve goes down from -45 to -70 ^{o} from 0.01 to 1 Hz and goes up continuously to ~30 at the frequency of 10^6 Hz. With the presence of magnetic field, the phase angle curve of MGNCs is almost stabilized at -60 until 3 Hz and then goes up continuously to the positive values.

References

1 B. R. V. Narasimhan, S. Prabhakar, P. Manohar, F. D. Gnanam, *Materials Letters* **2002**, *52*, 295.

2 L. B. Valdes, *Proceedings of the IRE* **1954**, *42*, 420.

3 F. G. de Souza Jr, B. G. Soares, J. C. Pinto, *European Polymer Journal* **2008**, *44*, 3908.

4 J. M. Miller, B. Dunn, *Langmuir* **1999**, *15*, 799.